A novel Deep Reactive Ion Etched (DRIE) glass micro-model for two-phase flow experiments

N.K. Karadimitriou[a], V. Joekar-Niasar[a], S.M. Hassanizadeh[a], P. J. Kleingeld[a], and L.J. Pyrak-Nolte[b]

[a] Utrecht University, Earth Sciences Department, Budapestlaan 4, 3584 CD, Utrecht, The Netherlands.

[b] Purdue University, Department of Physics, 525 Northwest Avenue, West Lafayette, Indiana 47907-2036, USA.

Abstract

In the last few decades, micro-models have become popular experimental tools for two-phase flow studies. In this work, the design and fabrication of an innovative, elongated, glass-etched micro-model with dimensions of 5 x 35 mm^2 and constant depth of 43 micron is described. This is the first time that a micro-model with such depth and dimensions has been etched in glass by using a dry etching technique. The micro-model was visualized by a novel setup that allowed us to monitor and record the distribution of fluids throughout the length of the micro-model continuously.

Quasi-static drainage experiments were conducted in order to obtain equilibrium data points that relate capillary pressure to phase saturation. By measuring the flow rate of water through the flow network for known pressure gradients, the intrinsic permeability of the micro-model's flow network was also calculated. The experimental results were used to calibrate a pore-network model and test its validity.

Finally, we show that glass-etched micro-models can be valuable tools in single and/or multi-phase flow studies and their applications.

1. Introduction

An efficient way to study two-phase flow in a porous medium is through the development of an artificial transparent porous medium with known properties, commonly referred to as "micro-model". An extensive review of micro-models use in two-phase flow studies (including fabrication methods and materials and visualization techniques) can be found in Karadimitriou and Hassanizadeh[1].

Up to now, most micro-models that have been used to study flow and transport in porous media are small domains of square, or nearly square, dimensions[2-7]. Therefore, one may interpret them as being one Representative Elementary Volume (REV). An REV is the volume of a homogeneous porous medium above which the system properties are

insensitive to the averaging domain's size. In this work, an elongated, glass-etched micro-model with dimensions 5x35 mm^2 was manufactured. The pore network was designed such that the REV size was around 5×7 mm^2. So, our micro-model was considered to be five times the REV size. The REV size was determined through pore-network modeling. Simulations were run for the whole extent of the micro-model. Then, capillary pressure-saturation curves were obtained for a sequence of gradually increasing sub-domain sizes and compared to each other. The subdomain size beyond which the capillary pressure-saturation curve remained unchanged was considered to be the REV.

In the work of Naga Siva et al.[8], the micro-fluidic device was also elongated, but it was made of two different materials. The flow network was created in a silicon substrate, and the whole model was sealed with a glass slide. This was needed because silicon is translucent and the model had to have a transparent side so that it could be visualized. However, that created a mixed-wettability system with undesirable and uncontrolled effects in two-phase flow processes.

In this work, we describe the design and fabrication of an elongated all-glass Deep Reactive Ion Etched (DRIE) micro-model. We have replicated a flow network that on average has the properties of an oil rock reservoir in a microfluidic chip. Comparative studies between pore-network modeling and micro-model experiments of the same flow network were made in order to investigate the efficiency of the use of such micro-models in two-phase flow studies. Properties of the flow network, such as intrinsic permeability, the relationship between phase saturation and capillary pressure, as well as phase flow rates, were measured and modeled.

The advantages of this micro-model were the following. First, the micro-model had a uniform wettability given that it is made of one material, namely glass. Second, the micro-model was totally transparent. In this way, direct optical visualization was made possible with the use of an innovative optical setup that will be described later.

To the best of our knowledge, this is the first time that two-phase flow studies are performed with such a uniformly wetting and elongated microfluidic glass chip with realistic pore sizes. The optical setup is also a breakthrough in real-time visualization methods for elongated samples.

2. Pore-network model description

The pore network was represented by an assembly of pore bodies (large pores) connected to each other by smaller pores, called pore throats. The pore network

topology was generated using Delaunay triangulation, as it is considered to provide a good representation of a real porous medium[9]. In Delaunay triangulation, points are connected to their neighbors by non-intersecting bonds. Connected points form triangles that are as equilateral as possible. The coordinates of the triangulation points were generated in MatLab. These points were considered to be the centers of the pore bodies. The overall dimensions of the network were 5 x 35 mm^2. In figure 1, the image of the whole network, as well as a magnified part of it, are shown.

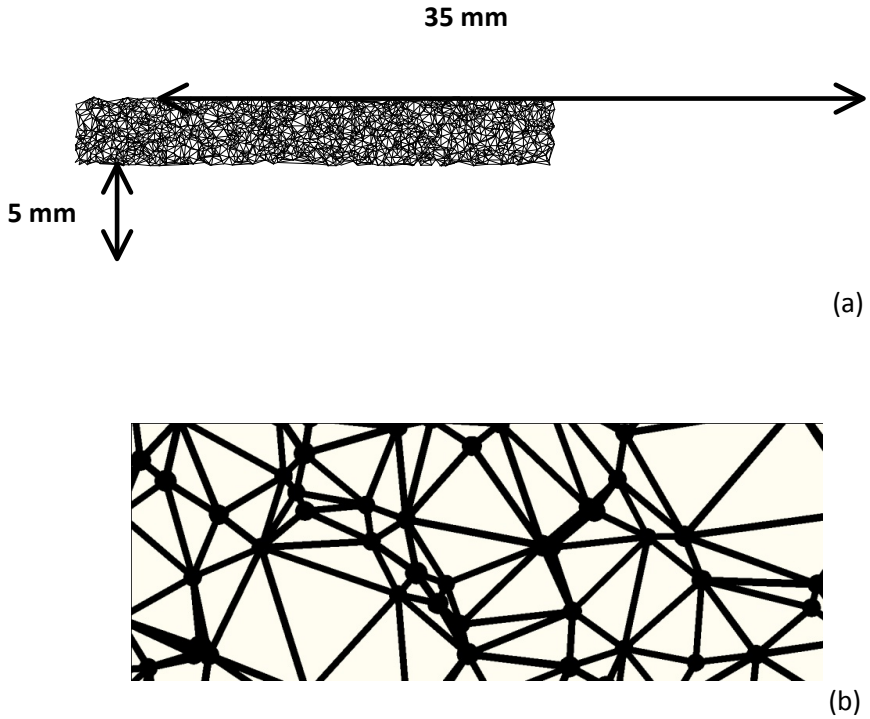

Figure 1. (a) Image of a pore-network with 2000 pore bodies and 6000 pore throats and a mean pore size of 70 μm. The void space is shown in black. (b) Zoom-in image of the network.

The pore network had a quasi-three-dimensional nature. It comprised a two-dimensional network of pores, but each pore was a three-dimensional element as it had a depth. The pore bodies had a cylindrical shape (they were circular in planar view; see Figure 1b) while pore throats had a parallelepiped shape (i.e, rectangular in planar view). Both pore bodies and pore throats had a rectangular cross-section. The SEM image of a typical cross section is shown in Figure 7. The coordination number, which is the number of connections of a pore body, varied from 4 to 6, depending on the total number of pore bodies.

The sizes of pore bodies were assigned from a truncated log-normal distribution. The mean pore size was selected to be equal to 70 μm. This value was selected in order for the visualization setup to be effective, as it will be explained later.

The length of a pore throat was defined as the distance between the centers of the neighboring pore bodies, *d*, minus the sum of their radii. The width of a pore throat was assigned such that it would always be smaller than the diameters of two neighboring pore bodies. This was given by a number of formulas used by Joekar-Niasar et al.[10].

Special attention was paid to the fact that the statistical distribution of sizes for pore bodies and pore throats should overlap to some extent, as this is the case in real porous media[11-13]. The depth of the network was chosen to be constant and close to the mean pore size.

3. Experimental setup and procedure

3.1 Micro-model

In the introduction of this manuscript, a general description of the micro-model was given. In the following sections, some more details are given regarding the construction of the micro-model.

3.1.1 Flow network

As mentioned earlier, the micro-model's flow network was exactly the same as the one that was used for numerical simulations. With the use of LISP[14] the network was converted to an Autocad sketch. Two reservoirs were added the same sketch and connected to the ends of the flow network. The Autocad sketch was then used for the production of a mask that was needed for the etching process.

3.1.2 Construction of the micro-model

In order to construct a glass-etched micro-model with DRIE, a chromium mask had to be prepared first (Compugraphics Intl. Ltd, Scotland). The mask was made of a glass plate coated with a thin layer of chromium. The flow network and the two reservoirs were created in the chromium layer. Areas of the mask that corresponded to the void space were transparent, while the rest was covered by chromium. In order to increase

the efficiency of the procedure and the maximum achievable depth, a layer of photoresist was applied on the glass slide in which the micro-model was to be created. First, the flow network was etched in the photoresist layer, over its full thickness, with the use of photo-lithography as an intermediate step[15,16]. Then, the glass slide was etched and flow network and the two reservoirs were created in it.

The pore network was printed on the by a laser-printing equipment at a resolution of 0.7 micron/pixel, which is quite high. It was essential for the resolution of the mask to be much higher than the resolution of our visualization setup. In this way, the rasterization of the mask would not be visible within the features of the flow network.

The etching was done using the Deep Reactive Ion Etching (DRIE) method[17-19]. This method was chosen as it is very accurate. Also, because it is highly anisotropic, it provides almost vertical walls. This was essential for the needs of the visualization setup, as explained shortly. However, there are some known issues (fabrication limits, accuracy of the process, etc.) with the maximum achievable depth[20,21]. In our case, we achieved a depth of 43 μm; this is the first reported microfluidic device made of glass with such a large depth.

Inflow and outflow reservoirs were also etched in the glass plate containing the flow network. They were etched with the use of wet-etching techniques and not with DRIE method, as the needs for detail were relaxed. A second glass plate was used to cover and seal the model with the help of chemicals and a large mechanical pressure. At the center of each reservoir, a hole was drilled in the cover glass plate for the introduction and removal of fluids.

The micro-model shown in Figure 2 has 3000 pore bodies and 9000 pore throats with a mean pore size of 70 μm. This micro-model was used to perform the experiments.

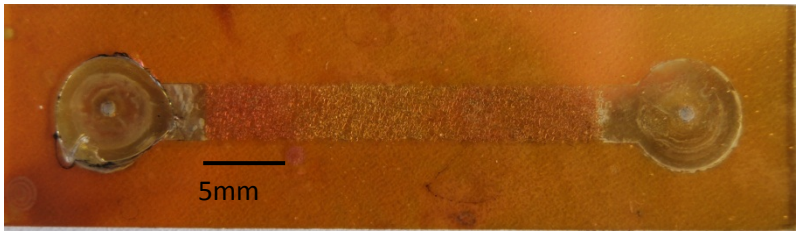

Figure 2. Picture of a micro-model with 3000 pore bodies and 9000 pore throats with a mean pore size of 70 μm. The two round reservoirs and the holes for introduction and removal of the two fluids are visible too.

3.2 Flow Visualization.

In most micro-model studies, a microscope has been used for visualization and a camera for recording images. As explained before, the main objective of this work was to design and fabricate an elongated micro-model for the study of two-phase flow under dynamic as well as quasi-static conditions. So, it was important for the visualization setup to allow simultaneous monitoring of flow throughout the whole micro-model as a function of time. For this reason, the use of a microscope was not applicable. The observation frame of a microscope is usually square. The smallest dimension of the object under observation and the required resolution always determine the size of this frame. In our case, the smallest dimension of the micro-model was the 5 mm. For the results of image processing to be reliable, the resolution had to be such that the smallest feature in the flow network could be visualized with at least 10 pixels. . Given that the narrowest throat had a width of 28 μm, the resolution of the visualization setup had to be at least 2.8 μm/pixel. This meant that only a frame of 5 x 5 mm^2 could be visualized, without being able to monitor the rest of the micro-model. One option would be to move the camera or the microscope. However, this procedure would take time, so the images obtained would not refer to the same time frame. Also, it would take too much time to process these images in order to eliminate any overlapping. Moreover, the movement of the model could introduce new, unknown forces that would affect the fluids distribution. For this reason, an alternative visualization method had to be developed.

3.2.1 Visualization setup

To visualize the whole micro-model, an innovative optical setup had to be designed and materialized. This setup involved an optical table, a collimated light source, a prism, an objective lens with a long focal length, three beam splitters, four cameras, and a computer for data acquisition. A schematic representation of the visualization setup can be seen in figure 3, with a photo shown in figure 4.

A beam splitter splits a light beam into two identical perpendicular ones. In theory, the intensity of the two beams would be half the intensity of the initial one. In practice, the intensity of the two beams was close to 47% of the initial value, due to energy losses in the beam splitter.

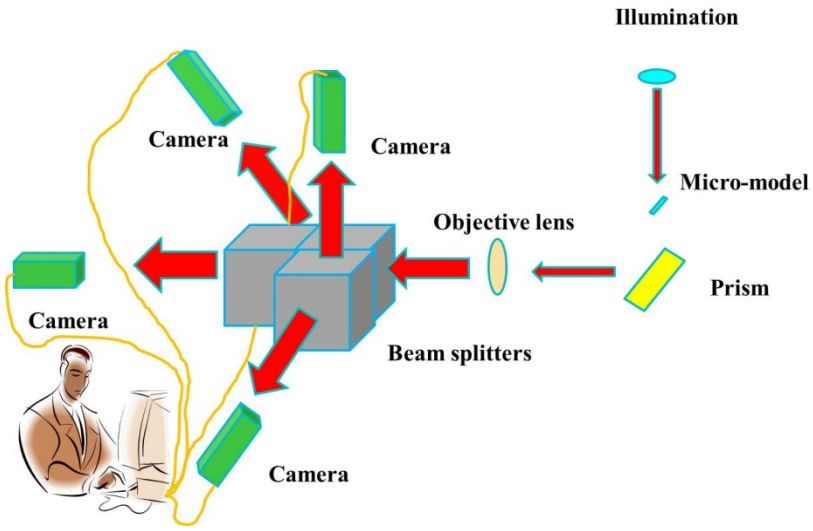

Figure 3. Schematic representation of the visualization principle of the experimental setup.

As shown in figure 3, a LED light source with tunable intensity emitting at 570 nm (*Jenoptik*) was used as the illumination source. The light source was put exactly at the focal point of a lens that had a focal length of 135 mm with respect to infinity. This arrangement provided a highly collimated light beam, at least for our working distance, with a diameter of 50 mm. This light beam, after passing through the glass micro-model, passed through a prism, so that its orientation would become parallel to the optical table. A Zeiss Sonnar T135mm f/1.8 ZA objective lens with a focal length of 135 mm was used to magnify the image. Right after the objective lens, three beam splitters (*Edmund Optics*) were combined in a way that they gave four identical reproductions of the initial light beam. The beam splitters were cubic with a side length of 35 mm. They were put inside a black box and their sides were covered with black paper in order to prevent internal reflections that would produce "ghost" images. These four images were captured by four GC-2450 Prosilica Ethernet cameras at a resolution of 5 Mpixels. The cameras were connected to a computer through Ethernet cables for data acquisition. They could record sequential pictures at a rate of 15 frames per second at the maximum resolution. By eliminating some lines from the sensor with the use of the appropriate software, the frame rate could reach 18 frames per second. The cameras were positioned such that they were focusing on four sequential parts of the initial image, visualizing most of the micro-model's length.

The design of this setup and the magnification was based on the micro-model size, the size of the camera sensor, and the requirement that the width of the smallest pore throat should be at least 10 pixels long. This meant that a minimum resolution of 2.8

μm/pixel was needed. Given the fact that the actual pixel size of the sensor of a GC-2450 camera is 3.45 μm, the magnification factor of the optical setup had to be 1.25. Thus, the initial size of the micro-model of 5 x 35 mm^2 would become 6.25 x 43.75 mm^2 after magnification. Given that the actual size of the sensor of each camera was 7.072 x 8.445 mm^2, a total area of 7.072 x 33.78 mm^2 could be monitored simultaneously at a resolution of 2.8 μm/pixel by the four cameras. That was 80% of the whole length of the micro-model. With a small compromise of reducing the resolution to 3.0 μm/pixel, an even bigger area could be covered, close to 85% of the total area.

The fact that the objective lens had an external filter diameter of 77 mm and a maximum aperture of f/1.8 provided the ability to produce images with minimal aberration and uniform light intensity. Its focal length of 135 mm provided the needed space for position the cameras within the boundaries of the optical table.

3.3 Pressure measurement and control

The micro-model was placed on a stage and it was directly connected to two external reservoirs, one for each phase. At exactly the same level as the level of the micro-model, two pressure transducers were installed to measure the pressure in the reservoirs. These transducers were connected to the controlling unit of a Bronkhorst differential pressure controller. The differential pressure controller had an RS-232 interface that was connected to a computer. In this way, it was possible to set, measure, and control the differential pressure between the two reservoirs at any instant. The controller was calibrated in a way that at its maximum span, the measured pressure would be 35 kPa with an accuracy of 35 Pa. The pressure controller was used to adjust the pressure in the non-wetting phase reservoir by increasing or decreasing the flow delivered to the non-wetting phase reservoir. . By increasing the pressure of the non-wetting phase reservoir, drainage could be initiated. The pressure in the wetting phase reservoir was always atmospheric.

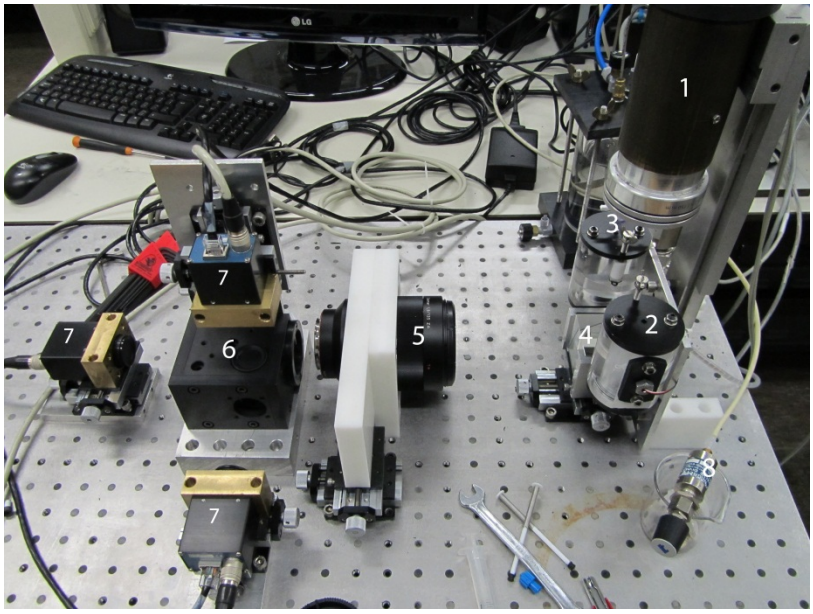

Figure 4. The experimental setup: 1) illumination, 2) wetting phase reservoir, 3) non-wetting phase reservoir, 4) prism, 5) lens, 6) box with beam-splitters, 7) cameras, 8) leak valve. There is another camera behind the box with the beam splitters that cannot be seen from this angle.

3.4 Two-phase displacement experiments

For our displacement experiments, dyed water was used as the wetting phase, and Fluorinert FC-43 as the non-wetting phase. The interfacial properties of dyed water and fluorinert, such as interfacial tension and contact angle, were measured. The interfacial tension between dyed water and fluorinert was found to be 55 mN/m, and the contact angle was 26 degrees. The dye was added to the water for increasing the optical contrast between the two phases and their easy identification in the images. In our preliminary experiments, the model was initially filled with the wetting phase. Drainage was initiated by gradually increasing the non-wetting phase pressure incrementally until it entered the micro-model. After each pressure step, the system was left for 20 minutes to reach equilibrium. Incremental pressure increase and the invasion of the non-wetting phase were continued until it reached the end of the model.

4. Results

During displacement experiments, images of the micro-model were acquired at various times and stored. In this part of the study, only equilibrium results were analyzed. In figure 5, sequential images taken from part of the network are shown.

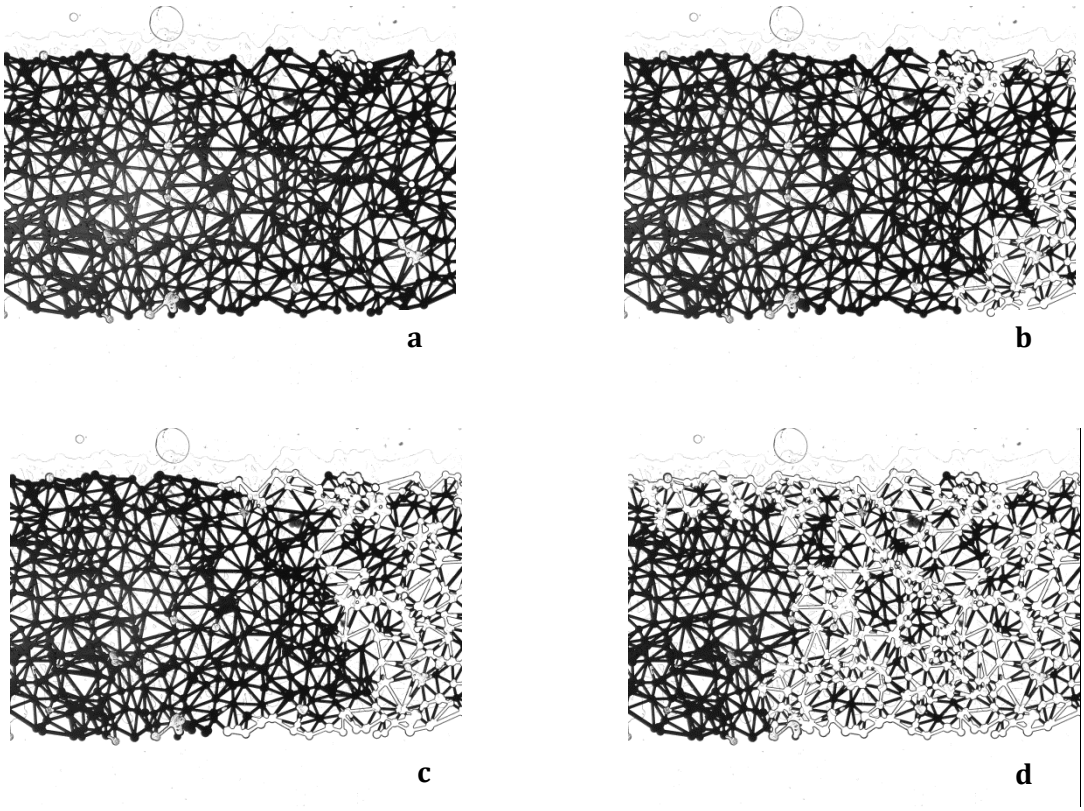

Figure 5. Images obtained from the micro-model during drainage. Initially the model is filled with the wetting phase (shown in dark color). Drained model at three sequential equilibrium states (b), (c), and (d). The non-wetting phase is shown in light color.

After image processing and calculation of average saturation, and with the use of the recorded values of the applied pressure, the P_c-S curve for drainage could be constructed. In figure 6, the measured data are shown along with the results obtained from the pore-network model for the same flow network. Results showed satisfactory agreement.

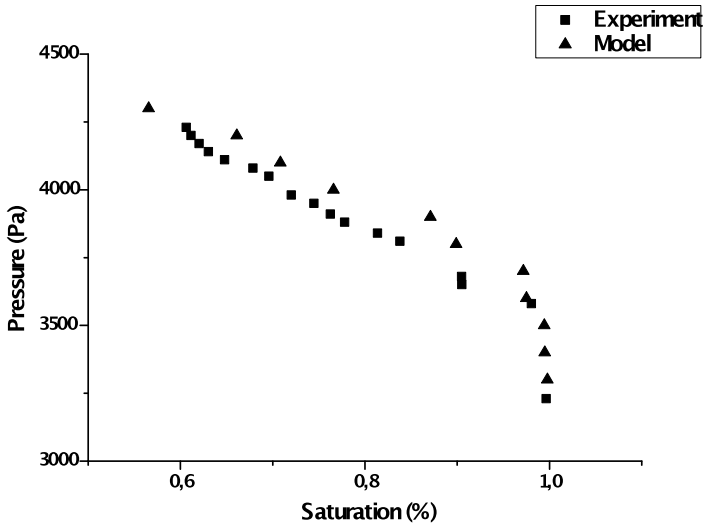

Figure 6. Pc-S data obtained from the experiment and the numerical model.

In order to measure the intrinsic permeability of the network, water was introduced into the micro-model at an imposed pressure. With the use of a Bronkhorst flow meter, the corresponding flow rate was measured at the outlet of the micro-model. Then with the use of Darcy's law[22] for single-phase flow, equation 1, K_{in} could be calculated

$$\vec{q} = -\frac{K_{in}}{\mu} \cdot (\vec{\nabla} P - \rho \vec{g}) \quad (1)$$

By repeating this measurement for different applied pressures and the corresponding flow rates, a mean value for the intrinsic permeability of the network was calculated, and found to be equal to Kin=6.10-12 m^2.

5. Discussion and Conclusions

In this work, a novel Deep Reactive Ion Etched, micro-fluidic device made of glass, with a depth of 43 μm, pre-defined properties, and suitable for single and/or multi-phase flow studies, was presented.

The data that were obtained experimentally for the P_c-S curve for the micro-model with 3000 pore bodies and 9000 pore throats, and a mean pore size of 70 μm, were compared to those obtained from the simulation for the same flow network. Intrinsic permeability was also calculated as an extra means of validating the correspondence between the experiment and the numerical model.

The comparison between the experimental results and the results obtained by the numerical model showed that there was a very good agreement between them. P_c-S curves collapsed onto each other, and the value obtained for intrinsic permeability was accurately estimated by the numerical model.

We observed that at a wetting-phase saturation of around 60%, all measured data points fell on top of each other. This happened because drainage was fully developed as soon as the non-wetting phase broke through the network. Additional drainage was not possible because the remaining wetting phase existed in isolated domains. However, in the numerical model the system was allowed to be fully drained.

Despite the fact that DRIE is highly anisotropic and can produce vertical walls, when the depth becomes large, for instance more than 20 μm, the walls become slightly sloped. This is visible in SEM images shown in figure 7.

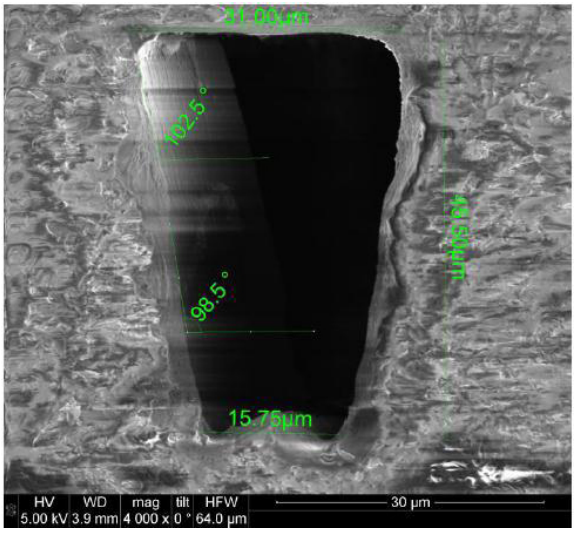

Figure 7. A SEM image showing the cross section of a pore throat formed in the micro-model.

In addition to the wall slope, the bottom surfaces of the channels were not smooth. In order to account for this slope and the roughness of the bottom and top surface in the numerical model, the parameters that affected the size distribution have been accordingly tuned. The slope on the walls of the network channels introduced some problems in the visualization efficiency. When there is a slope on the walls, light that comes from the illumination source gets refracted and never reaches the camera's sensor. As a result, the two-dimensional projection of the slope appeared in black. Given that the slope was not high, its effect was not significant in the visualization setup.

The displacement of two fluid phases in the model could be directly visualized and recorded as a function of time. The agreement between the results obtained from micro-model experiments and pore-network model simulations were satisfactory. This agreement verified that a glass micro-model with uniform properties is a useful tool for studying and understanding two-phase flow processes.

References

1. Karadimitriou, N. K., and Hassanizadeh, S. M. (2012), A review of micro-models and their use in two-phase flow studies, *Vadose Zone Journal*, accepted for publication.
2. Pyrak-Nolte, L. J., D. D. Nolte, D. Chen, and N. J. Giordano (2008), Relating capillary pressure to interfacial areas, *Water Resour. Res*., **44**, W06408, doi:10.1029/2007WR006434.
3. Berejnov, V., Djilali, N., and Sinton, D., (2008), Lab-on-chip methodologies for the study of transport in porous media: energy applications, *Lab Chip*, **8**, pp. 689–693.
4. Tsakiroglou, C.D., and Avraam, D.G. (2002), Fabrication of a New Class of Porous Media Models for Visualization Stuies of Multiphase Flow Process, J. of Material Sci., 37, 353.
5. Chen, D., L. Pyrak-Nolte, J. Griffin, and N. Giordano (2007), Measurement of interfacial area per volume for drainage and imbibition, *Water Resour. Res*., **43**, W12504, doi:10.1029/2007WR006021.
6. Chen, L., and Kibbey, T. C. G. (2006), Measurement of Air–Water Interfacial Area for Multiple Hysteretic Drainage Curves in an Unsaturated Fine Sand, *Langmuir*, **22** (16), pp. 6874–6880, doi: 10.1021/la053521e.
7. Cheng, J.-T., L. J. Pyrak-Nolte, D. D. Nolte, and N. J. Giordano (2004), Linking pressure and saturation through interfacial areas in porous media, *Geophys. Res. Lett*., **31**, L08502, doi:10.1029/2003GL019282.
8. Naga Siva, G., Bera, B., Karadimitriou, N. K., Mitra, S. K., and Majid Hassanizadeh, S. M., (2011), Reservoir-on-a-Chip (ROC): A new paradigm in Reservoir Engineering, Lab Chip, DOI:10.1039/C1LC20556K, 2011
9. Heiba, A., Sahimi, M., Scriven, L., and Davis, H. (1992), Percolation theory of two-phase relative permeability, *SPE Reserv. Eng*., **7**, pp. 123–132.
10. Joekar-Niasar, V., Hassanizadeh, S. M., Dahle, H. K. (2010), Non-equilibrium effects in capillarity and interfacial area in two-phase flow: Dynamic pore-

network modeling", *Journal of Fluid Mechanics*, doi:10.1017/S0022112010000704.

11. Al-Raoush, R. I., Willson, C. S. (2005a), Extraction of physically realistic pore network properties from three-dimensional synchrotron X-ray microtomography images of unconsolidated porous media systems, *Journal of Hydrology*, Vol. **300**, Issues 1-4, pp. 44-64, ISSN 0022-1694, DOI: 10.1016/j.jhydrol.2004.05.005.
12. Al-Raoush, R. I., Willson, C. S. (2005b), A pore-scale investigation of a multiphase porous media system, *Journal of Contaminant Hydrology*, Vol. **77**, Issues 1-2, pp. 67-89, ISSN 0169-7722, DOI: 10.1016/j.jconhyd.2004.12.001.
13. Joekar-Niasar, V., S. M. Hassanizadeh, and A. Leijnse (2008), Insights into the relationships among capillary pressure, saturation, interfacial area and relative permeability using pore-scale network modeling, *Transp. Porous Media*, doi:10.1007/S11242-007-9191-7.
14. McCarthy, J.; Brayton, R.; Edwards, D.; Fox, P.; Hodes, L.; Luckham, D.; Maling, K.; Park, D. (1960), LISP I Programmers Manual. Boston, Massachusetts: Artificial Intelligence Group, M.I.T. Computation Center and Research Laboratory, Accessed May 11, 2010.
15. Thompson, L.F., C.G. Wilson and M.J. Bowden (1983), Introduction to Microlithography, ACS Symp. Ser., 219.
16. Thompson, L. F., C. G. Willson, and M. J. Bowden (1994), Introduction toMicrolithography, 2nd ed., Am. Chem. Soc., Washington, D. C., doi: 10.1002/pi.1995.210370312.
17. Blauw, M. A., T. Zijilstr, and E. van der Drift (2001), Balancing the etching and passivation in time-multiplexed deep dry etching of silicon, *J. Vac. Sci. Technol*. *B*, **19**, pp. 2930-2934.
18. Willingham, T. W., Werth, C. J., and Valocchi, A. J. (2008), Evaluation of the Effects of Porous Media Structure on Mixing-Controlled Reactions Using Pore-Scale Modeling and Micromodel Experiments, *Environmental Science & Technolog*, **42** (9), pp. 3185-3193.
19. Yeom, J., Y. Wu, and M. A. Shannon (2003), Proceedings of Transducers '03-The 12th International Conference on Solid State Sensors, Actuatorsand Microsystems, IEEE, Boston, MA, p. 1631.
20. Yeom, J., Y. Wu, J. C. Selby, and M. A. Shannona,(2005), Maximum achievable aspect ratio in deep reactive ion etching of silicon due to aspect ratio dependent transport and the microloading effect, *Journal of Vacuum Science & Technology B:*

Microelectronics and Nanometer Structures, **23**: 6, pp. 2319 – 2329,1071-1023.doi:10.1116/1.2101678.

21. Ohara, J., Asami, K., Takeuchi, Y. and Sato, K. (2010), Development of RIE-lag Reduction Technique for Si Deep Etching Using Double Protection Layer Method, IEEJ Transactions on Electrical and Electronic Engineering, 5: 125–130. doi: 10.1002/tee.20506.
22.

Darcy, H. (1856), Les Fontaines Publiques de la Ville de Dijon, Dalmont, Paris.